Available online at www.sciencedirect.com
ScienceDirect
Journal of Nuclear Materials 356 (2006) 16–26
journal of nuclear materials
www.elsevier.com/locate/jnucmat

Development of resistant materials to beam impact and radiation damage ☆

Masayoshi Kawai [a,*], Hiroyuki Kokawa [b], Hiroshi Okamura [b], Akira Kawasaki [b], Tsutomu Yamamura [b], Nobuyoshi Hara [b], Noboru Akao [b], Masatoshi Futakawa [c], Kenji Kikuchi [c]

[a] *Institute of Materials Structural Science, High Energy Accelerator Research Organization, 1-1 Oho, Tsukuba-shi 305-0801, Japan*
[b] *Graduate School of Engineering, Tohoku University, 6-6-02 Aramaki-aza-Aoba, Sendai 980-8579, Japan*
[c] *Japan Atomic Energy Agency (JAEA), Tokai-mura, Ibaraki-ken 319-1195, Japan*

Abstract

Materials that have strong resistance to both beam impact (or shock-wave) and radiation damage are required for the beam target of an intense accelerator and space applications. Recently, Futakawa et al. found in their experiments that Kolsterising specimens have a stronger resistance to pitting than SS316 CW. A similar effect can be expected for other hardening treatments, and new material development is hopeful. Accordingly, we have started the development of high-performance materials by organizing the project team from KEK, JAEA and universities. In this paper, the scope of the project is introduced. Recent topics involve the development of intergranular crack (IGC)-resistant austenitic stainless-steel, AlN–TiN ceramics and cladding techniques of thin tantalum or CrN film on a tungsten target by means of a molten-salt method and ion-beam-enhanced deposition. New observations on corrosion resistance are presented.

1. Introduction

Materials which have strong resistance to both beam impact (or shock-wave) and radiation damage are required for the beam target of an intense accelerator and space applications. Recently, spallation target engineering groups discovered pitting damage under the pulsed irradiation of liquid–metal targets [1], and have studied the phenomenon and counter measures. Futakawa et al. [2] derived the following observation in their pitting experiments for total impact cycles above one million: Kolsterising specimens have a stronger resistance to pitting than SS316 CW. A similar effect can be expected for other hardening treatments, and new material development is hopeful. Recently, we have organized a project team to develop high-performance materials that are strong against shock-waves and radiation.

☆ The present work has been made by the high performance material developing team under the support by 2004–2006 Grand-in-Aid for Science Research (A) by JSPS.
* Corresponding author. Tel.: +81 298 64 5637; fax: +81 298 64 3202.
E-mail address: masayoshi.kawai@kek.jp (M. Kawai).

0022-3115/$ - see front matter © 2006 Elsevier B.V. All rights reserved.
doi:10.1016/j.jnucmat.2006.05.021

The team is composed of scientists from KEK, JAEA and universities (Tohoku, Kyoto, Hokkaido, Kobe, Kyushu and Okayama University of Science).

The project scope is as follows:

(1) Development of new materials and cladding techniques by means of grain boundary engineering (GBE), powder metallurgy to make functionally gradient materials and new ceramics, surface treatment with nitriding and laser peening etc., and surface coating with electro-deposit using molten-salt and the PVD method etc.
(2) Evaluation of newly developed materials, such as microscopic observations with TEM/SEM, neutron, synchrotron orbital radiation (SOR) and positron, mechanical tests and residual stress measurements by neutrons, impact tests with high-speed camera observations, post-irradiation experiments for the STIP-2 samples for tungsten alloys, ion-beam irradiation tests and FEM analyses for impact tests, thermal stress etc.

The desired material generally has a high yield stress and high hardness as well as resistance to corrosion and radiation. A method other than Kolsterising is to create new materials using powder metallurgy, combined with mechanical alloying and heat processes etc. Cladding is also promising to use for tantalum-clad tungsten targets and coating on aerospace parts. However, the coating or cladding technique has a weak point of breaking a coat or flaking off the base material at the interface, because of the joint of the two different materials. In some cases, the coating film thickness becomes very important. In such cases, we will estimate the film thickness for materials to achieve the desired lifetime by a computer simulation technique using an FEM. Functionally gradient materials seem to be ideal, since there is no abrupt change at the interface and the shock-wave will be gradually absorbed through transmitting a mixture layer. Electro-chemical deposition in molten-salt seems to be attractive to improve the surface properties of materials. To investigate the effects of radiation damage, we will perform measurements of STIP-II samples Moreover, we will simulate irradiation testing with ion- and electron-accelerators.

In the present paper, recent topics are introduced.

2. Topics

2.1. Grain boundary engineering

In constructing a structure, welding is required. Intergranular corrosions, resulting in weld decay, is frequently observed in the heat affected zone (HAZ) of austenitic stainless-steel. The weld decay region is located in the HAZ of the welded specimen of an as-received 304 steel plate, as schematically illustrated in the upper part of Fig. 1. The optical micrograph of the weld decay region in the lower part of Fig. 1 shows a mixed structure of grooved and non-grooved boundaries by 10% oxalic acid electro-etching [3]. IGC is initially caused by $Cr_{23}C_6$ precipitation in the grain boundary. Chromium carbide precipitation leads to sensitization by chromium depletion. Such sensitization can not be perfectly prevented only by previous conventional techniques, such reducing the carbon content, a stabilization-treatment, a local solution-heat-treatment, etc. Recent studies on the grain boundary structure have revealed that the sensitization depends strongly on the crystallographic nature and the atomic structure of the grain boundary, and that low-energy grain boundaries, such as CSL (coincidence site lattice) boundaries, have strong resistance to intergranular corrosion [4]. The concept of 'grain boundary design and control' [5] has been developed through GBE [6] to inhibit sensitization by increasing the frequency of CSL boundaries. GBEed materials, which are characterized by high frequencies of CSL boundaries, are resistant to intergranular deterioration of materials, such as intergranular corrosion [7–9]. In the present work, Kokawa of Tohoku University tried to produce a GBEed austenitic stainless-steel possessing a strong resistance to weld decay using an identical 304 steel.

2.1.1. Experimental

A commercial type-304 austenitic stainless-steel was used throughout this study. The chemical composition (wt%) was 18.28 Cr, 8.48 Ni, 0.60 Si, 1.00 Mn, 0.055 C, 0.029 P and 0.005 S. A base material plate of $9 \times 50 \times 150$ mm^3 was welded by bead-on-plate gas-tungsten-arc (GTA) welding at a welding current of 300 A in direct current electrode negative (DCEN), a travel speed of 4 cm/min, and an arc length of 1 mm without filler materials in a welding chamber filled with argon gas.

For a thermomechanical treatment to perform GBE, the initial size of the base material specimen

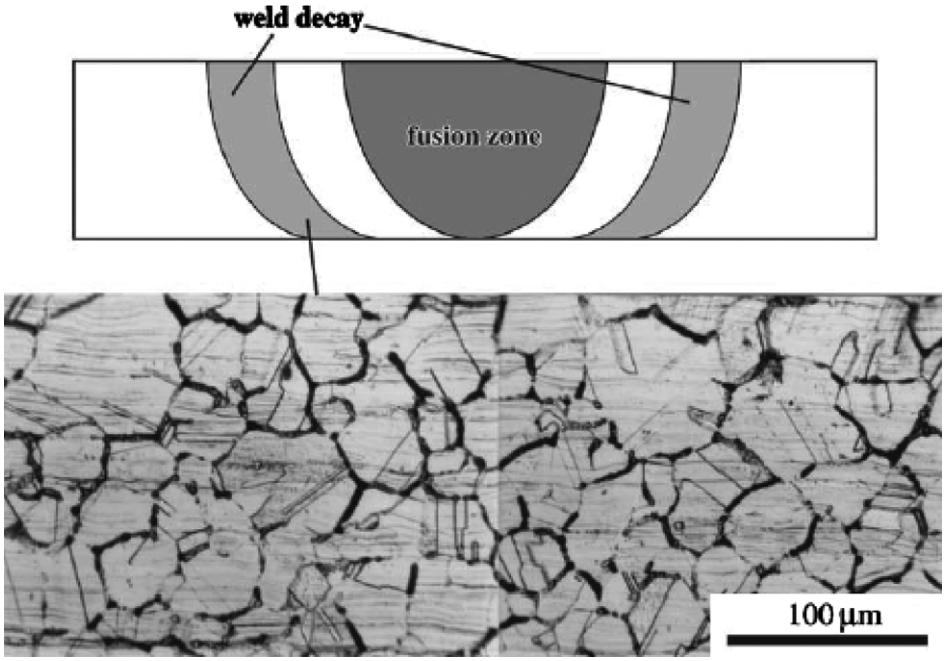

Fig. 1. Mixed structure of grooved and non-grooved boundaries in the weld decay region of the weld-HAZ of the initial 304 austenitic stainless-steel after 10% oxalic acid electro-etching [3].

was $9 \times 10 \times 35$ mm^3. The specimens were solution-heat treated at 1323 K for 0.5 h. A thermomechanical treatment was performed by cold-rolling and subsequent annealing. The roll-reduction ratio in thickness resulted in as pre-strain from 0 to 60%. The pre-strained specimens were annealed at various temperatures from 1200 to 1600 K and quenched in cold water. The GBCD (grain boundary character distribution) was examined by OIM (orientation imaging microscopy). The intergranular corrosion resistance was evaluated by a double loop electro-chemical potentiokinetic reactivation (DL-EPR) test [10] after sensitization treatment at 923 K. The base material (BM) and 5% strain-annealed (r5%) specimens were assessed by a ferric sulfate–sulfuric acid test [11] after a sensitization at 923 K. The tested specimens were observed by SEM. The as-received and the GBEed (thermomechanically treated) materials of the 304 steel were GTA welded and the weld HAZs were observed by SEM and TEM, and examined by a corrosion test and OIM.

2.1.2. Optimum condition for GBE

Recently, Shimada et al. [12] have demonstrated that a slight pre-strain annealing at a relatively low temperature results in excellent intergranular corrosion resistance due to optimized GBCD in type-304 austenitic stainless-steel. The effects of the roll-reduction ratio as pre-strain on the reactivation current ratio during the DL-EPR test after the sensitization treatment and on the frequency of CSL boundaries in the thermomechanically treated 304 steel indicated an optimum pre-strain of 5% in strain annealing at 1300 K in the GBE process of this material. The effect of the annealing temperature at 5% pre-strain on the GBCD was examined by OIM. The annealing temperature and time were varied to find the process parameters needed to achieve the optimum GBCD. A favorable change in the GBCD was observed during annealing at 1200 K, i.e., with increasing annealing time at 1200 K; a high CSL frequency layer (about 85% CSL) was formed near the rolled surface and expanded into the specimen. The OIM indicates that the high CSL frequency area including random boundary debris remained in the surface layers, whereas a continuous random boundary network remained in the inner region. A uniform distribution of the high CSL frequency area was achieved in an r5% specimen annealed at 1200 K for 72 h (r5%-1200 K-72 h). A number of twins formed in the growing grains compensate grain-coarsening. The network of random grain boundaries in the

as-received base material was totally disrupted, and short random boundary segments were isolated in the r5%-1200 K-72 h specimen. The differences in GBCD between the BM, r5%-1300 K-0.5 h, r5%-1200 K-48 h and the r5%-1200 K-72 h specimens are schematically illustrated in Fig. 2.

2.1.3. Corrosion test

The DL-EPR test results reflect the fractional area of chromium depletion near sensitized grain boundaries on the test surface. The actual intergranular corrosion propagates along grain boundaries from the surface into the material, and causes mass-loss due to falling off the specimen surface. The corrosion (mass-loss) rate during the ferric sulfate–sulfuric acid test is shown in Fig. 3 for the BM, r5%-1300 K and r5%-1200 K specimens after sensitization. The strain-annealed specimens have much lower corrosion rates than the BM for every test duration. The difference in mass-loss is much more than that expected simply from differences in the DL-EPR test results and CSL boundary frequencies, because the improvement in GBCD can strongly affect the mass-loss. The r5%-1200 K-72 h specimen with the optimized GBCD (Fig. 2(d)) indicated the smallest corrosion rate, which was less than one-fourth that of the BM, and less than half that of the r5%-1300 K-0.5 h specimen.

2.1.4. Effect of GBE

In order to examine the effect of GBE on the weld decay in 304 austenitic stainless-steel, the r5%-1200 K-72 h specimen with the optimized GBCD and the as-received 304 base material were GTA-welded. The HAZ of each weld was observed after electro-etching in an oxalic acid solution. In the HAZ, distributed between 0 mm and 12 mm away from the fusion line (surface of the fusion zone of Fig. 1), of the as-received base material, most of the grain boundaries are grooved in the areas far away (about 8 mm) from the fusion line, as generally seen in weld decay. In contrast, almost none of grain boundaries are grooved through the HAZ of the GBEed material. Both the degree of sensitization by the DL-EPR test and the corrosion rate during the ferric sulfate–sulfuric acid test were much lower in the weld of GBEed material than in that of the as-received 304 steel base material [23].

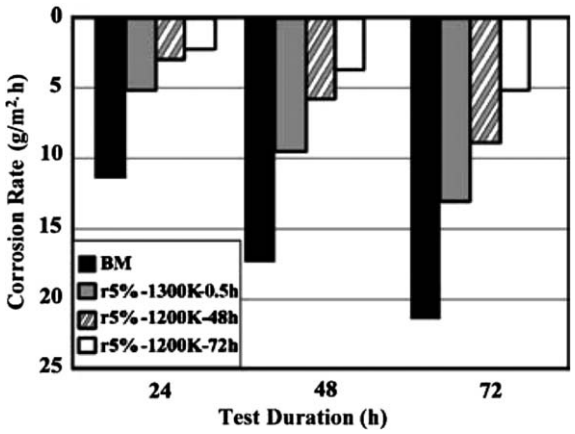

Fig. 3. Corrosion mass-loss of the BM and the strain-annealed specimens during a ferric sulfate–sulfuric acid test [12].

2.1.5. Summary

Grain boundary engineering was used to improve intergranular-corrosion and the weld-decay resistance

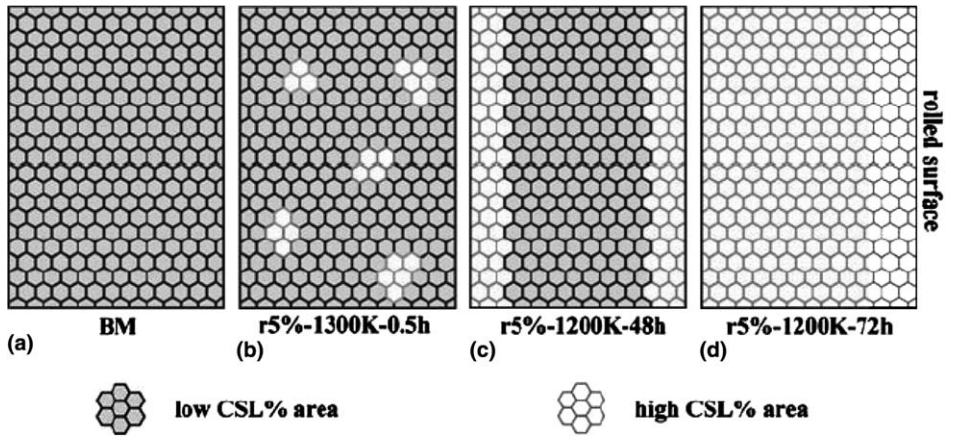

Fig. 2. Schematic illustration of the GBCD in the initial material (BM) (a), and thermomechanically treated specimens with different parameters (b), (c) and (d) [12].

of an austenitic stainless-steel. The sensitivity to intergranular corrosion was reduced by the thermomechanical treatment, and indicated a minimum at a small roll-reduction. The frequency of CSL boundaries indicated a maximum at the small roll-reduction. The corrosion rate in a ferric sulfate–sulfuric acid test was much smaller in the thermomechanical treated specimen than in the base material for long-time sensitization.

2.2. Preparation of TiN–AlN fine-grained ceramics composite

Titanium nitride (TiN) has been widely used as a coating of cutting tool because of its high hardness and low friction coefficient. In order to improve its toughness, composites of TiN and other ceramics, such as AlN or Al_2O_3 etc., have been studied. Among them, AlN is a promising candidate because of the notable difference between the thermal expansion coefficients ($9\times10^{-6}\,K^{-1}$for TiN, 4–6 $\times$ $10^{-6}\,K^{-1}$ for AlN), which may introduce thermal strain during cooling and thus can lead to the toughening of the composite. Moreover, the thermal conductivity of the composite is expected to increase due to the presence of AlN, which will be favorable to thermal shock-resistant applications. Recently, TiN–AlN composites have been prepared by H. Okamura and A. Kawasaki of Tohoku University using a mechanical alloying technique based on an in situ chemical reaction with NH_3 which was produced from the disintegration of ammonium carbonate during mechanical alloying:

$$Ti + NH_3 \rightarrow TiN$$ [13].

The microstructure and mechanical properties of the composite were investigated.

2.2.1. Experimental

Two different synthesis routes were employed with the same designed compositions (TiN:AlN = 1:1 (mole ratio)): one is to ball-mill AlN and TiN powders in ethanol (composite A). The other was TiN–AlN composite powders synthesized in situ from powders of AlN, Ti and ammonium carbonate as initial materials, by taking advantage of the chemical reaction between Ti and ammonium carbonate during 32 h mechanical alloying and a heat treatment of heating at 1200 °C for 2 h. Synthesized powders were pressed by 100 MPa into a green pellet and CIP'ed at 200 MPa (composite B). X-ray diffraction showed that Ti in the composite B diminished through a 32 h-milling and 2 h-heating process. In both cases, HIP was made under the condition of 1750 °C, 180 MPa for 2 h as a sintering process in order to obtain full-densified bulk materials. The microstructure was observed with SEM and TEM. Vickers hardness and fracture toughness were measured by the indentation method.

2.2.2. Results

Considerably fine powder of below 50 nm was obtained by mechanical alloying with the following parameters: 32 h-milling of AlN, Ti and ammonium carbonate as shown in Fig. 4. The values of the Vickers hardness and fracture toughness are compared in Table 1. The values of composite B, which was prepared by mechanical alloying using AlN, Ti and ammonium carbonate, are higher than those of both composite A, which was prepared by ball-milling of AlN and TiN powders, and TiN. A microstructural observation showed that different phases were mixed by nano-scale in composite B, while they were mixed by a scale of several micrometers in composite A. Fig. 5 shows that particle bridging and crack deflection occurred in composite B around indentations, which led to its higher toughness than composite A.

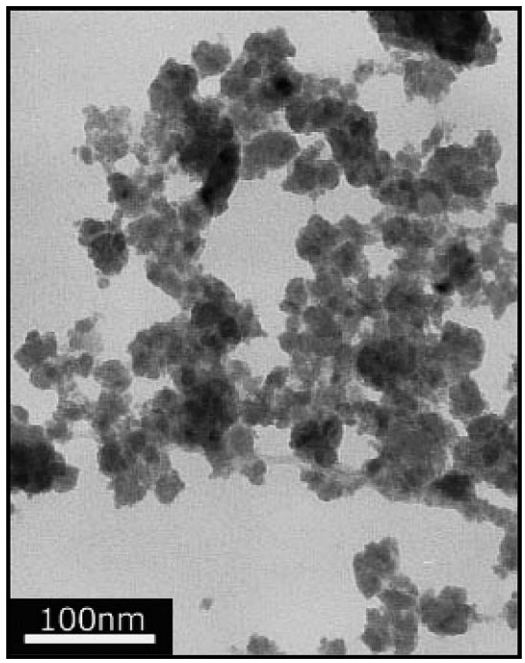

Fig. 4. TEM image of a mechanically alloyed powder (composite B).

Table 1
Comparison of the mechanical properties

Sample	Density (kg/m^3)	Hardness (GPa)	Toughness ($MPa/m^{1/2}$)
Composite B	4690	19.6	5.1
Composite A	4230	16.0	2.48
TiN	5260	12.1	3.9

A further investigation will be made to measure the material properties of the presently produced ceramics.

2.3. Ta cladding on tungsten by electro-deposition with a molten-salt bath method

Tantalum exhibits a high corrosion resistance over a wide range of aggressive media, but has weak points of reduced neutron production compared to tungsten and high decay heat resulting from high radio activities induced by thermal neutrons [14]. It will be required to minimize any decay heat for exchanging a used target into a new one by reducing the amount of tantalum-clad on tungsten. Electro-deposition is extremely useful due to high flexibility for big size complicated shape of the objects to be coated, and has an advantage of low cost. Molten-salt electrolysis has been successfully applied for the deposition of valve metals [15] and their alloys [16]. In the present work, Yamamura group of Tohoku University investigated two possibilities for the electro-deposition of tantalum on tungsten. One was to pre-coat an additional intermediate layer of nickel before a tantalum coating; the other was to coat on bare tungsten [17].

At first, a dense and compact coating of tantalum on nickel was pursued to attain a Ta coating on a tungsten substrate mediated by a thin Ni layer. The electrolyte consisted of 55%LiF–35%NaF–10%CaF_2 in which 1% K_2TaF_7 was added. (Percentage is given in mole percent.) The cell consisted of a graphite crucible. A nickel rod was used as a quasi-reference electrode (cathode) and a graphite rod was used as a counter electrode (anode). The electro-deposition was carried out at 700 °C under an argon atmosphere. A electro-deposition of tantalum on nickel wire (1-mm diameter) was performed at a current density of 0.2 kA m^{-2}. The result was shown at IWSMT-5 [18], which clearly revealed that a continuous and rather smooth coating on the nickel layer has been possible.

Additional attempts to prepare coatings directly on tungsten were performed. Electro-chemical measurements were performed by using a tungsten/nickel wire, a graphite rod and a nickel rod as the working, counter and quasi-reference electrodes, respectively. A graphite or nickel crucible was used. The electro-chemical measurements were performed at 700 °C under an argon atmosphere. When coating was attempted in a melt containing 2% K_2TaF_7 at low current densities, the quality of the interface improved significantly, although the deposit was found only on about 10% of the surface. This led us to the conclusion that the melt containing higher concentration of K_2TaF_7 affects the deposit at the initial stage of deposition, such that the regions with a poor interface are not formed, or dissolve away easily. The chronopotentiometry showed that the current efficiency increased at higher current densities. Hence, attempts were made to prepare coatings on tungsten at higher current densities, which proved to be successful, and complete coverage was obtained on tungsten. Fig. 6 shows a SEM image and an X-ray image of

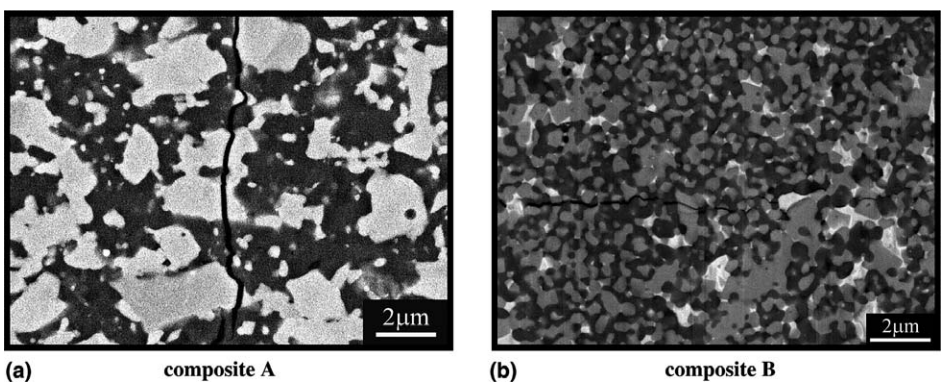

Fig. 5. Comparison of the indentation crack path for composite A and composite B.

tantalum after electroplating tantalum on tungsten at a current density of 1 kA m^{-2} in a melt containing 2% K_2TaF_7. It can be noticed that SEM does not reveal the interface. Accordingly, a rather good interface is formed by electroplating in the melt containing 2% K_2TaF_7.

In summary, the cladding of tantalum on tungsten is possible by electro-deposition in a LiF–NaF–CaF_2 melt containing 2% K_2TaF_7 at a current density of ~1–1.5 A m^{-2}.

2.4. CrN cladding on tungsten plate

Nio et al. [14] and Takenaka et al. [19] pointed out, based on their neutronics and thermal calculations on 0.5 mm thick-tantalum-clad tungsten target for MW class spallation neutron source, that there were severe problems of high gamma-ray dose and decay heat from activated tantalum during maintenance of the target. On the other hand, CrN has a high hardness and a high resistance against corrosion, wear and oxidization. Nio et al. also showed that CrN cladding would become a solution of problems involving a tantalum-clad tungsten target because CrN was much less activated compared to tantalum.

Since the surface properties of CrN film are likely depend on the film formation technique, we tried to make a CrN cladding on a tungsten plate with different techniques. One is an arc-plasma type PVD technique at Japan Coating Center Co. Ltd. and Japan ITF Co. Ltd. This method is very popular, and film formation process is standardized in the former company. The film thickness was controlled by the deposition time to be 5 μm and 8 μm. In Japan ITF Co. Ltd, the ion-plating processes were made twice and the film thickness was measured with a spherical abrasion test method to be 2.4 μm and 2.0 μm (total 4.4μm).

The other was ion-beam-enhanced deposition (IBED) at Tohoku University. In the IBED, a film was deposited on a substrate by the ion-beam sputtering of target material and, at the same time, the film was bombarded by another ion-beam source ~enhancement source. By this method, it was possible to increase the mobility of the depositing chemical species and cause reactions between the depositing film and the bombardment ions. It was therefore possible to control the composition and the structure of films by controlling ion-bombardment conditions and other deposition conditions. CrN*x*thin films were formed by the IBED method. A dual ion-beam sputtering apparatus was employed. Fig. 7 shows a schematic representation of the apparatus. The distances between the sputter source and the target, the target and the substrate, and the enhancement source and the substrate were 100, 130 and 180 mm, respectively. The incident angle of the sputter ion-beam to the target was 45°. The substrate was set parallel to the target. The incident angle of ion-beam from the enhancement source to the substrate was 9°. A high-purity Ar gas (purity 99.9999 vol.%) was used for the sputter source, and a high-purity Ar gas and a high-purity N_2 gas (purity 99.9999 vol.%) were used for the enhancement source. The base pressure of the vacuum chamber

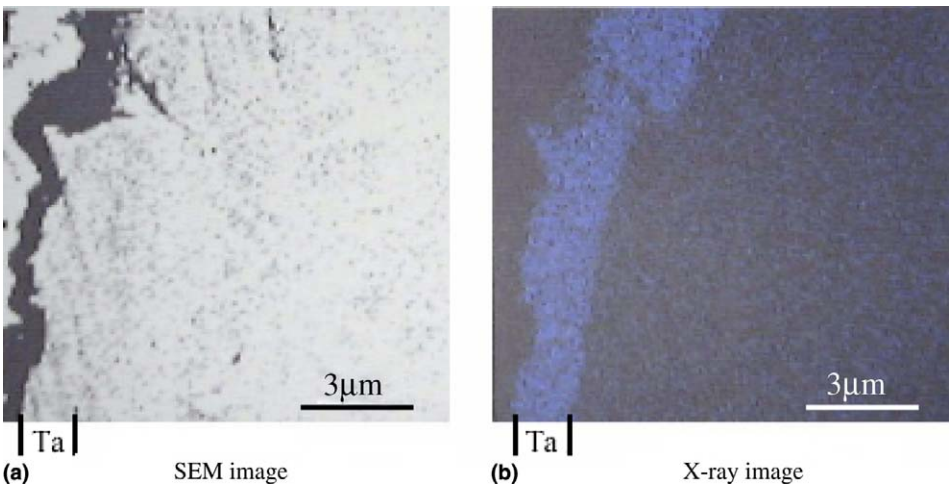

Fig. 6. Cross-sectional view of tungsten after electro-depositing tantalum at a current density of ~ 1 kA m^{-2}: (a) SEM image and (b) X-ray image of Ta.

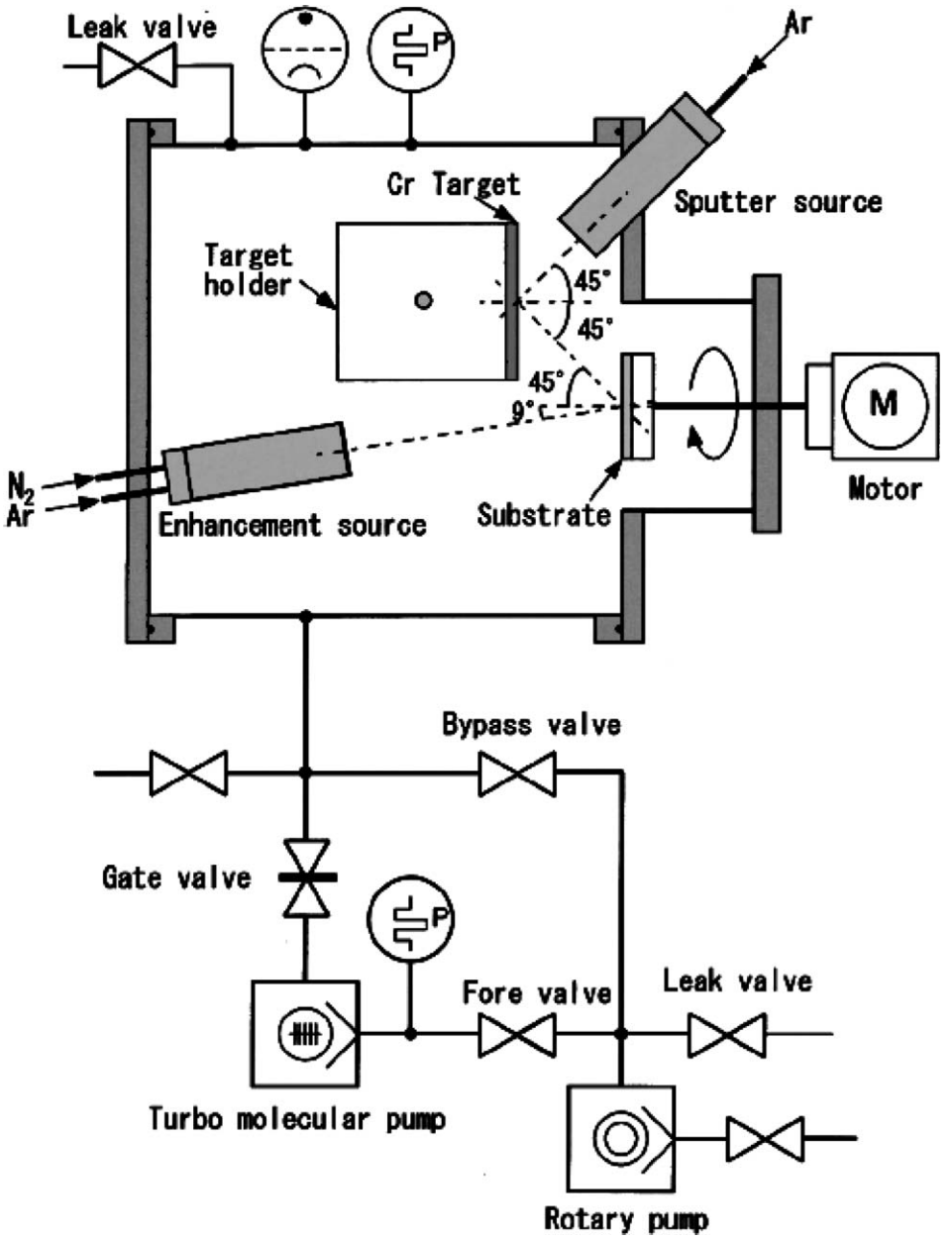

Fig. 7. Schematic representation of the apparatus used for ion-beam-enhanced deposition.

was less than 2.4×10^{-7} Torr, and the working pressure was 4.4×10^{-4}–4.6×10^{-4} Torr. A pure chromium plate (purity 99.9 mass%) of 120 mm × 120 mm × 4 mm was used for the target. Tungsten plates of 20 mm × 20 mm × 5 mm and tungsten disk of 20 m in diameter and 2 mm thickness were used as the substrates. Before the first deposition of CrN film, tungsten substrates were degrease in ultrasonically acetone.

In the IBED process, the sputter source was operated at a fixed condition, that is, a beam voltage of 600 V, an accelerator voltage of 100 V, a beam current of 13 mA, and an Ar gas flow rate of 4 sccm. The enhancement source was operated under the following conditions: a beam voltage of 200 V, an accelerator voltage of 600 V, a beam current of 20 mA, and an Ar and N_2 gas flow rate of 3.0 sccm and 5.0 sccm, respectively. This condition is to

produce the CrN thin film having the lowest pinhole defect density of 0.005% [20]. The beam current is determined by the discharge current, the accelerator voltage, and the total gas (Ar and N_2) flow rate. It is supplied to the source anode placed in the enhancement source. The accelerator voltage is applied on the accelerator grit, and the beam voltage is done on the source anode. Therefore, it is possible to control the energy and quantity of ions emitted from the enhancement source. The deposition time was 480 min.

The film thickness of the specimen produced with the IBED process was measured by a stylus-based surface profiler to be 350–400 nm. Fig. 8 shows a typical example of SEM photographs of specimen surface. The surface of the CrN thin film formed by IBED is very smooth, while that of the film formed by ion plating displays pronounced microparticles and pinhole-like defects.

CrN clad tungsten specimen are now being investigated concerning their microstructure, mechanical properties, irradiation effect by electrons, W-blistering effect by MeV proton irradiation and lifetime of target plate of 100 mm × 60 mm × 5 mm under thermal cycles compared with a tantalum-clad W-target plate that was fabricated by the HIP method [21]. An investigation of CrN cladding is also progressing by means of the molten-salt bath method at Kyoto University.

2.5. Properties of surface-treatment austenite steel

In a mercury target under pulsed-irradiation conditions, the pitting of the target vessel and the window from cavitation erosion is so severe that it can limit our ability to determine the lifetime of a target. Recent experiments clarified that the treatment to the surface to increase the hardness was effective for increasing the materials resistance against impact erosion. The following techniques can be applied for the surface treatment: kolsterize (*a registered trademark of Bodycote International plc.,*i.e., carbonate), nitride and cladding or film formation with hard materials such as TiN and CrN. Fig. 9 shows a comparison of the impact erosion resistances as a function of the hardness between the 316-type austenite stainless-steel and surface-treated materials [22]. Here, the impact erosion resistance is defined to be an inverse of fraction of the eroded area. It is strongly correlated with the hardness, as shown in the figure. Therefore, harder materials provide better resistance against pitting damage.

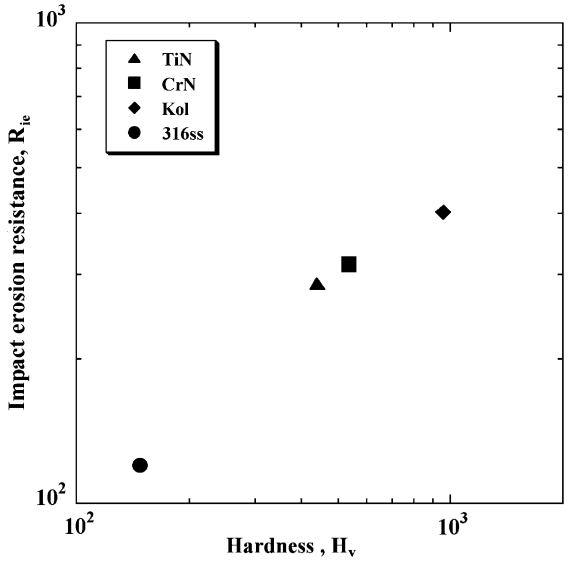

Fig. 9. Relationship between the hardness and impact erosion resistance.

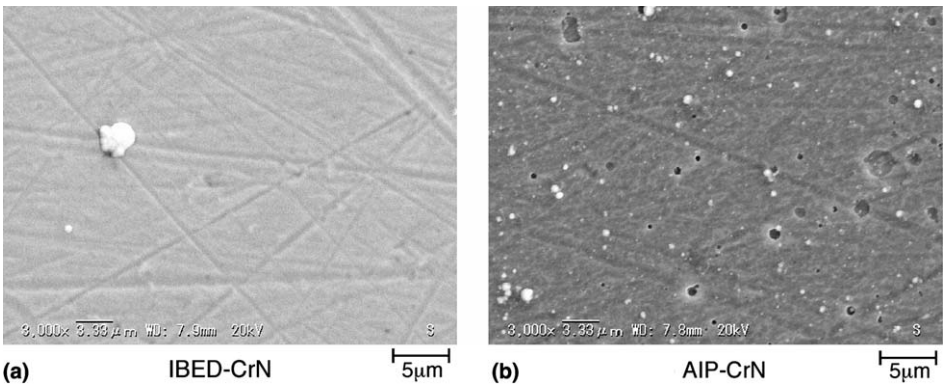

Fig. 8. Comparison of SEM photographs of CrN clad tungsten plates.

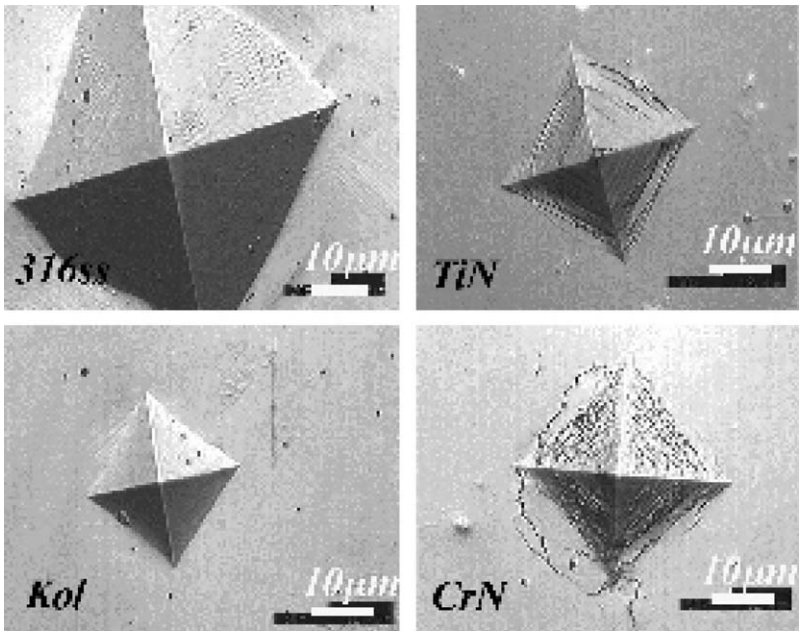

Fig. 10. Micrographs of indents at 4.9 N.

However, if the pitting damage penetrates through a hard material, which is obtained by a surface-treatment, damage will abruptly proceed. In addition, these surface may be less ductile. Accordingly, the layer thickness will be limited. Recently, Futakawa et al. measured the hardness of materials as a function of the indent thickness, and found that it decreased with the depth in the case of surface-treatment materials, while austenite stainless-steel did not have such a thickness dependence of the hardness. The surface of a micro-Vickers-hardness-tested specimen was observed, as shown in Fig. 10. In the case of a TiN and CrN clad material, we can observe a micro-cracks around the indentation at 4.9 N. Accordingly, the impact erosion resistance against multi-cycle (beyond 10^8 cycles) stresses depends not only on the hardness, but also on the bond strength between the coating and the base material. Accordingly, a complex structure of hard materials/stick materials/substrate may be promising for impact erosion.

3. Summary

We are investigating ways to develop materials that have strong resistance against impact shock and irradiation for spallation targets and aerospace. There are five topics reported as a result of recent activities. One topic is the development of the GBE-treated steel that has high resistance to IGC. Such a material is expected to have high resistance to IASCC. The second is the development of new ceramics of AlN–TiN with a nano-structural technique using a chemical reaction in situ during mechanical alloying. The developed material is 1.6-times harder than TiN. The third is the formation of CrN cladded tungsten plates with different methods, including ion plating and ion-beam enhanced deposition. A thin tantalum-cladded tungsten specimen has been prepared with an electro-deposition technique in a molten-salt bath. Finally, the relationship of impact erosion to the material properties has been studied.

In the next stage, material development and characterization will be promoted. As for material development, cladding or film coating on SS is needed by using a more improved method, such as laser peening, as well as an optimized condition, even for the conventional method. Presently, CrN film formation with the molten-salt method is being performed at Kyoto University. Functionally graded materials are much promising for impact erosion resistance and aerospace applications.

The characterization of materials and the material behavior under impact condition is very important to develop new materials as well as computer simulations with modern sophisticated models. Instantaneous phenomena will be observed under

impact shock. Material observations will be made with not only conventional tools of materials and mechanical properties, but also by quantum beam diffraction methods using X-ray and neutrons. For example, the residual stresses of thermo-mechanical treated or impacted materials will be measured using neutrons and X-rays. As for radiation damage, the GBE materials will be supplied to the STIP experiments and JMTR irradiation tests. Ion and electron bombardment experiments are made for CrN-coated tungsten to investigate the blistering effect and dislocation behavior. Thermal cycle tests will be made for clad W target plates.

References

[1] K. Kikuchi, H. Kogawa, M. Futakawa, S. Ishikura, K. Kaminaga, R. Hino, J. Nucl. Mater. 318 (2003) 84.
[2] M. Futakawa, T. Naoe, C.C. Tsai, H. Kogawa, S. Ishikura, Y. Ikeda, H. Soyama, H. Date, J. Nucl. Mater. 343 (2005) 70.
[3] H. Kokawa, M. Shimada, Y.S. Sato, JOM 52 (2000) 34.
[4] P. H. Pumphrey, in: G. A. Chadwick, D. A. Smith (Eds.), Grain Boundary Structure and Properties, Academic Press, London, 1976, p. 139.
[5] T. Watanabe, Res. Mechanica 11 (1984) 47.
[6] G. Palumbo, E.M. Lehockey, P. Lin, JOM 50 (1998) 40.
[7] E.M. Lehockey, G. Palumbo, P. Lin, A.M. Brennenstuhl, Scripta Mater. 36 (1997) 1211.
[8] E.M. Lehockey, G. Palumbo, P. Lin, Metall. Mater. Trans. A 29 (1998) 3069.
[9] P. Lin, G. Palumbo, K.T. Aust, Scripta Mater. 36 (1997) 1145.
[10] A.P. Majidi, M.A. Streicher, Corrosion 40 (1984) 584.
[11] J.B. Lee, Corrosion 39 (1983) 469.
[12] M. Shimada, H. Kokawa, Z.J. Wang, Y.S. Sato, I. Karibe, Acta Mater. 50 (2002) 2331.
[13] M. Krasnowski et al., Nanostruct. Mater. 12 (1999) 455.
[14] D. Nio, M. Ooi, N. Takenaka, M. Furusaka, M. Kawai, K. Mishima, Y. Kiyanagi, J. Nucl. Mater. 343 (2005) 163.
[15] S. Senderoff, G.W. Mellors, W.J. Reinhart, J. Electrochem. Soc. 8 (1965) 266.
[16] M. Mohamed, N. Kawaguchi, Y. Sato, T. Yamamura, J. Alloys Compound. 287 (1999) 91.
[17] M. Mehmood, N. Kawaguchi, H. Maekawa, Y. Sato, T. Yamamura, M. Kawai, K. Kikuchi, Electro-deposition of tantalum on tungsten and nickel in LiF–NaF–CaF2 melt containing K2TaF7, Electrochemical Study Material Transactions 44-2 (2003) 259.
[18] M. Kawai, M. Furusaka, K. Kikuchi, H. Kurishita, R. Watanabe, J.-F. Li, K. Sugimoto, T. Yamamura, Y. Hiraoka, K. Abe, A. Hasegawa, M. Yoshiie, H. Takenaka, K. Mishima, Y. Kiyanagi, T. Tanabe, N. Yoshida, T. Igarashi, J. Nucl. Mater. 318 (2003) 38.
[19] N. Takenaka, D. Nio, Y. Kiyanagi, K. Mishima, M. Kawai, M. Furusaka, J. Nucl. Mater. 343 (2005) 169.
[20] H. Kondo, N. Akao, N. Hara, K. Sugimoto, J. Electrochem. Soc. 150 (2) (2003) B60.
[21] M. Kawai, M. Furusaka, J.F. Li, A. Kawasaki, T. Yamamura, M. Mehmood, H. Kurishita, K. Kikuchi, N. Takenaka, Y. Kiyanagi, T. Igarashi, M. Katoh, Solid spallation target materials development, in: Proceedings of Sixteenth Meeting of the International Collaboration on Advanced Neutron Sources, May 12–15, 2003, Düsseldorf-Neuss, Germany, ESS 03-136-M1, vol. 3, p. 1087.
[22] M. Futakawa, H. Kogawa, R. Hino, H. Date, H. Takeishi, Int. J. Imp. Eng. 28 (2003) 123.
[23] H. Kokawa, J. Mater. Sci. 40 (2005) 927.